




## Article

# Low-Cost High-Performance SnO<sub>2</sub>–Cu Electrodes for Use in Direct Ethanol Fuel Cells

Hany S. Abdo <sup>1,2</sup> , Amit Sarkar <sup>3</sup>, Madhu Gupta <sup>3</sup>, Suvadra Sahoo <sup>4</sup>, Jabair A. Mohammed <sup>1</sup> , Sameh A. Ragab <sup>1</sup> and Asiful H. Seikh <sup>1,\*</sup> 

- <sup>1</sup> Center of Excellence for Research in Engineering Materials, King Saud University, Riyadh 11421, Saudi Arabia; habdo@ksu.edu.sa (H.S.A.); jmohammed@ksu.edu.sa (J.A.M.); sragab@ksu.edu.sa (S.A.R.)
- <sup>2</sup> Mechanical Design and Materials Department, Faculty of Energy Engineering, Aswan University, Aswan 81521, Egypt
- <sup>3</sup> Department of Metallurgical Engineering, Jadavpur University, Kolkata 700032, India; amitsarkar553@gmail.com (A.S.); mdhugpta@gmail.com (M.G.)
- <sup>4</sup> Metallurgical and Material Engineering Department, Veer Surendra Sai University of Technology, Sambalpur 8062, India; subhadrasahoo007@gmail.com
- \* Correspondence: aseikh@ksu.edu.sa; Tel.: +966-559204166

**Abstract:** The high cost of Pt-based electrode materials limits the commercialization of fuel cells and their subsequent application in renewable energy production. It is thus necessary to develop economical, high-performance electrodes alongside biofuels to reduce the pollution associated with the production of energy. Tin dioxide–copper foil (SnO<sub>2</sub>–Cu) electrode materials are herein developed using an electrodeposition process. Cyclic voltammetry, chronoamperometry, and potentiodynamic polarization methods are used to electrochemically characterize the electrode materials, with the results revealing that their excellent catalytic properties result in them delivering a high current. The surface morphologies of the developed electrodes are examined using scanning electron microscopy, with the results showing that upon an increase in the deposition time, a finer deposit of SnO<sub>2</sub> is formed on the surface of the Cu foil. Consequently, electrochemical oxidation using an enhanced surface area of the material leads to it exhibiting a high current and excellent corrosion resistance. Powder X-ray diffraction was used to confirm the successful depositing of SnO<sub>2</sub> on the surface of Cu. The fuel cell fabricated using the SnO<sub>2</sub>–Cu electrode is promising for use in clean energy generation, as it can be prepared at low cost compared to conventionally used electrodes.

**Keywords:** electrochemical characterization; high energetic electrodes; cyclic voltammetry; chronoamperometry; ethanol fuel cell



**Citation:** Abdo, H.S.; Sarkar, A.; Gupta, M.; Sahoo, S.; Mohammed, J.A.; Ragab, S.A.; Seikh, A.H. Low-Cost High-Performance SnO<sub>2</sub>–Cu Electrodes for Use in Direct Ethanol Fuel Cells. *Crystals* **2021**, *11*, 55. <https://doi.org/10.3390/cryst11010055>

Received: 17 December 2020

Accepted: 8 January 2021

Published: 11 January 2021

**Publisher's Note:** MDPI stays neutral with regard to jurisdictional claims in published maps and institutional affiliations.



**Copyright:** © 2021 by the authors. Licensee MDPI, Basel, Switzerland. This article is an open access article distributed under the terms and conditions of the Creative Commons Attribution (CC BY) license (<https://creativecommons.org/licenses/by/4.0/>).

## 1. Introduction

Tin dioxide (SnO<sub>2</sub>) is a key material used in photovoltaic cells, lithium batteries, and gas sensors [1–5]. The most widely used methods to make deposits of SnO<sub>2</sub> are spin coating [6], electrodeposition [7], evaporation [8], chemical vapor deposition [9,10], sol–gel processes [11,12], and the pyrolysis of tin compounds [13]. Due to it requiring a low temperature and the high energy that can be generated near electrode surfaces, electrodeposition is an effective process for synthesizing powders and coating films and can be used to prepare complicated surfaces. This technique has been commonly used to prepare metal-based coatings since before 1900 on account of it being inexpensive in terms of both raw materials and equipment. Over the last few decades, metal oxides have also been successfully prepared via electrodeposition [14–19]. Moreover, nowadays, it is easy to synthesize films that have excellent properties by controlling the electrodeposition parameters, materials, and synthesis conditions.

The capacity of SnO<sub>2</sub> is approximately double that of graphite, making it one of the most important anodic materials used in fuel cell applications. In 2002, Chang et al. [20]

successfully synthesized nanocrystalline SnO<sub>2</sub> via cathodic electrodeposition, which is one of the most effective ways of fabricating nanosized SnO<sub>2</sub> and is an ideal method for use in industrial applications because of the unlimited choices in terms of substrate materials that can be used during deposition [21,22]. Therefore, in this study, cathodic electrodeposition was selected as the method of choice for producing nanosized SnO<sub>2</sub>. As OH<sup>−</sup> ions or O<sup>−</sup> radicals are required in the electrodeposition of metal oxides, an oxygen source is a necessity. Several oxygen sources have been reported to be effective in the cathodic electrodeposition of metal oxides, such as blown oxygen gas, hydrogen peroxide, and nitrate ions [23–25].

As is known, when the grain or particle size of a metal oxide is refined to the nanoscale, the chemical and physical properties of the compound change significantly, depending on the new nanocrystalline structure generated upon its reduction in size. Due to the excellent performance of nanometal oxides, the research in this area has progressed, leading to materials with excellent properties being reported for use in nanotechnology [26–30].

In this study, SnO<sub>2</sub> is deposited on copper (Cu) foil via cathodic electrodeposition over various time periods. The surface morphologies of the coated films are studied using scanning electron microscopy (SEM). Film characterization and phase identification of the deposited layers are performed using powder X-ray diffraction (PXRD). Electrochemical characterization of the developed SnO<sub>2</sub> deposits on Cu foil is achieved using cyclic voltammetry (CV), chronoamperometry, and potentiodynamic polarization methods.

## 2. Experimental

### 2.1. The Pre-Treatment of Materials and Chemicals

Cu foil with a surface area of 1 cm<sup>2</sup> was polished using emery papers of different grades, then washed using distilled water, and dried using a high-pressure air jet. The foil was then washed using dilute acetic acid to remove any Cu oxide [16]. After washing it with distilled water, the Cu foil was then immersed in acetone for 15 min to remove any organic impurities or contaminations, followed by cleaning with both methanol and distilled water for a further 15 min.

SnO<sub>2</sub> electrodeposition on a Cu electrode was carried out via a two-electrode set-up using a potentiostatic route involving 20 mL of SnCl<sub>4</sub>·5H<sub>2</sub>O (99% purity, from Sigma Aldrich, St. Louis, MO, United States). Comparing electrode set-ups, the three-electrode system is much more stable than a two-electrode system because of its accuracy in measuring the voltage, however, in large-scale production and industrial applications, two-electrode systems are more commonly used. In the two-electrode system used in this work, a 1 cm<sup>2</sup> Cu plate was used as the cathode and a graphite electrode as the anode, separated by a distance of around 28 mm. During all electrodeposition experiments, the electrolyte was stirred continuously using a low speed stirrer and after each experiment the cathodes were cleaned using distilled water, before being dried under a jet of air. The electrodeposition process was repeated three times for different time periods of 10, 15, and 20 min.

### 2.2. Electrochemical Characterization

To study the electrochemical performance of the developed electrodeposited samples, chronoamperometry, CV, and potentiodynamic polarization techniques were used employing a pH 13.1 1 M ethanol + 1 M potassium hydroxide (KOH) solution.

The CVs of the electroplated samples were measured using a computer controlled electrochemical framework machine, DY 2300 potentiostat, and a three-electrode system. The working anode was the sample to be measured, with a graphite rod and saturated calomel electrode (SCE) employed as counter and reference electrodes, respectively. The tests were conducted using a stepping potential at a scan rate of 50 mV/s in the range of −1.3–0.3 V vs. SCE at the open circuit potential to calculate  $I_{\max}$  (current efficiency).

Chronoamperometry ( $I$  vs.  $t$ ) was performed on the above-mentioned equipment using different software, in which to ascertain the time taken for the current to be transmitted from the cell, the current ( $I$ ) was analyzed as a component of time ( $t$ ). Trial tests

were carried out at various potentials to determine the ethanol oxidation potential of the electrode materials.

Potentiodynamic polarization tests on all the samples were carried out at room temperature in 1 M ethanol + 1 M KOH solution at a scan rate of 1 mV/s using a Gamry potentiostat (PC/750, Warminster, PA, USA), where SCE and graphite were used as reference and counter electrodes, respectively, and the sample to be tested was employed as the working cathode. As the surface area exposed to the solution differs according to the sample being assessed, a standardized sample area was considered for all of the samples when plotting the data.

The above-mentioned three-electrode Gamry potentiostat system was also used for electrochemical impedance spectroscopy (EIS) measurements. The EIS tests were performed in the frequency range of 0.1 Hz–30 kHz with a signal amplitude of 10–20 mV. At each frequency, the absolute impedance and phase angles were measured to obtain data for a Nyquist plot, in which the impedance data were interpreted and fit to an appropriate equivalent electrical circuit using a simplex fit model, involving both real and imaginary data components.

### 2.3. Physical Characterization

The samples were characterized using PXRD and SEM. PXRD patterns were collected at room temperature using a Rigaku Ultima III X-ray diffractometer equipped with a monochromatic Cu K $\alpha$  source operated at a scan rate of 2°/min. Peak analysis of the data was carried out using the inbuilt software of the diffractometer.

Microstructural characterization and surface morphology determination of the samples were carried out by SEM using a JEOL JSM 6360 microscope.

## 3. Results and Discussions

### 3.1. Cyclic Voltammetry Study

Figure 1 shows the CV curves of the SnO<sub>2</sub>-coated Cu foil samples electrodeposited for different time periods at a fixed temperature in 1 M ethanol + 1 M KOH solution, where it can be seen that for all the curves, there is a current maximum representing the highest rate of ethanol oxidation, at which point the maximum output current is delivered from the anode compartment of the fuel cell. It is interesting to note that the SnO<sub>2</sub>-coated Cu foil that was electrodeposited for 20 min exhibits the maximum current. According to the information in the literature [17,31,32], the point corresponding to conditions where the rate of nucleation is the highest and the rate of growth is the lowest gives rise to finer and nano deposits.

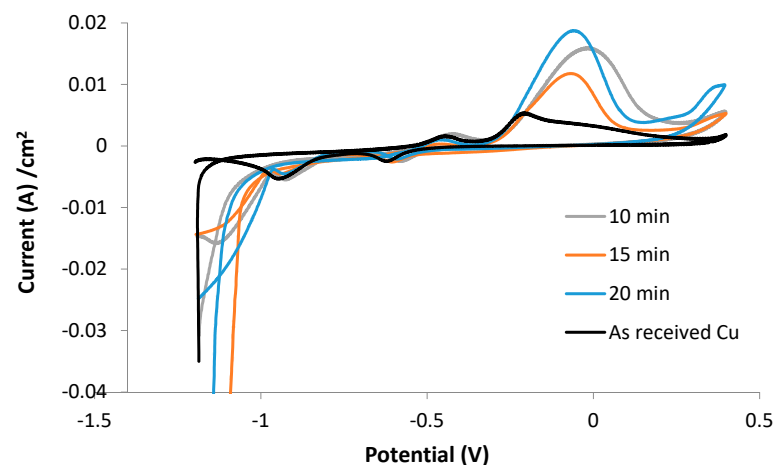


**Figure 1.** CV curves of the as-received Cu foil (black line) and the SnO<sub>2</sub>-coated Cu foil samples deposited over different times periods of 10 min (green line), 15 min (red line), and 20 min (blue line) recorded in 1 M ethanol + 1 M potassium hydroxide (KOH) solution.

### 3.2. Chronoamperometry Study

Chronoamperometry is a technique that is useful for determining the steady state current of a sample after investigation, especially after observing a high current peak, as was determined in the CV data of the SnO<sub>2</sub>-Cu electrodes. Figure 2 shows the chronoamperometry results of the electrocoated SnO<sub>2</sub>-Cu samples prepared at different deposition times recorded in 1 M ethanol + 1 M KOH solution. From the data, it can be seen that the currents associated with the samples initially follow a downward trend before reaching steady state values, around which they generally remain for the duration of the experiments. This data shows that SnO<sub>2</sub> is a promising electrode material for use in fuel cell applications. It can also be observed that the SnO<sub>2</sub> sample deposited for 20 min exhibited the highest current in the chronoamperometry results, as well as the highest peak in the CV measurements.

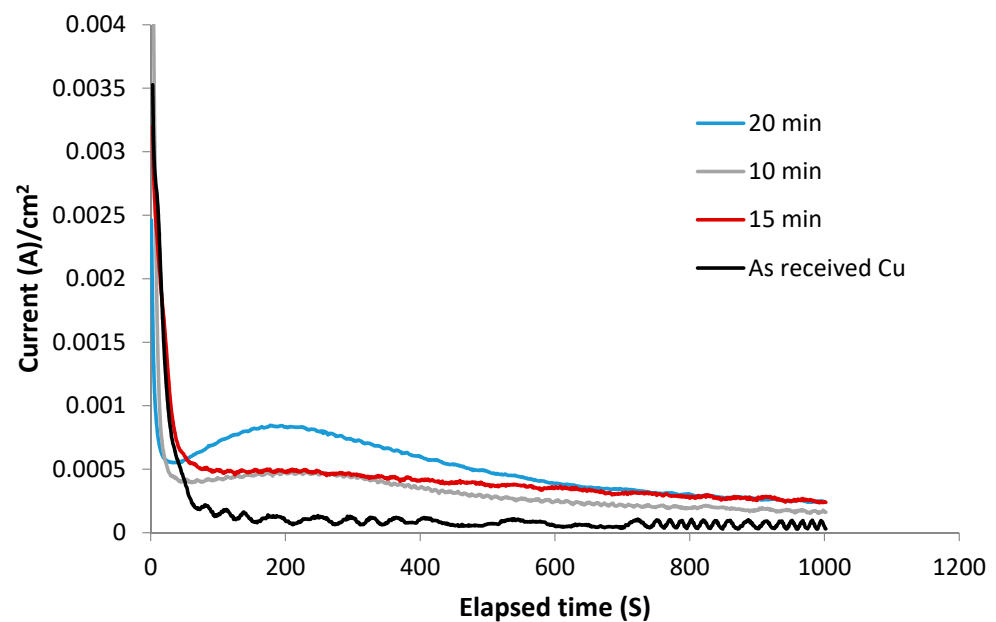


**Figure 2.** Chronoamperometry curves of the ethanol oxidation reaction on as-received Cu foil (black line) and the SnO<sub>2</sub>-coated Cu foil samples deposited over different times periods of 10 min (green line), 15 min (red line), and 20 min (blue line).

### 3.3. Potentiodynamic Polarization Analysis

Potentiodynamic polarization tests were carried out on the prepared SnO<sub>2</sub>-coated Cu electrodes to determine their electrokinetic properties. Figure 3 shows the polarization curves of the as-received Cu foil and SnO<sub>2</sub>-coated Cu electrodes recorded in 1 M ethanol + 1 M KOH solution. Table 1 shows the data obtained from the polarization curves using the Tafel extrapolation method. It can be clearly seen from the curves that the sample deposited over the longest time period of 20 min exhibits a higher current density than the other samples, indicating that the current delivery from the electrodes increases in line with an increase in the deposition time. The corrosion current density values,  $i_{\text{corr}}$ , also show the same trend, and there is not much difference between the corrosion potential values,  $E_{\text{corr}}$ , of all of the samples.

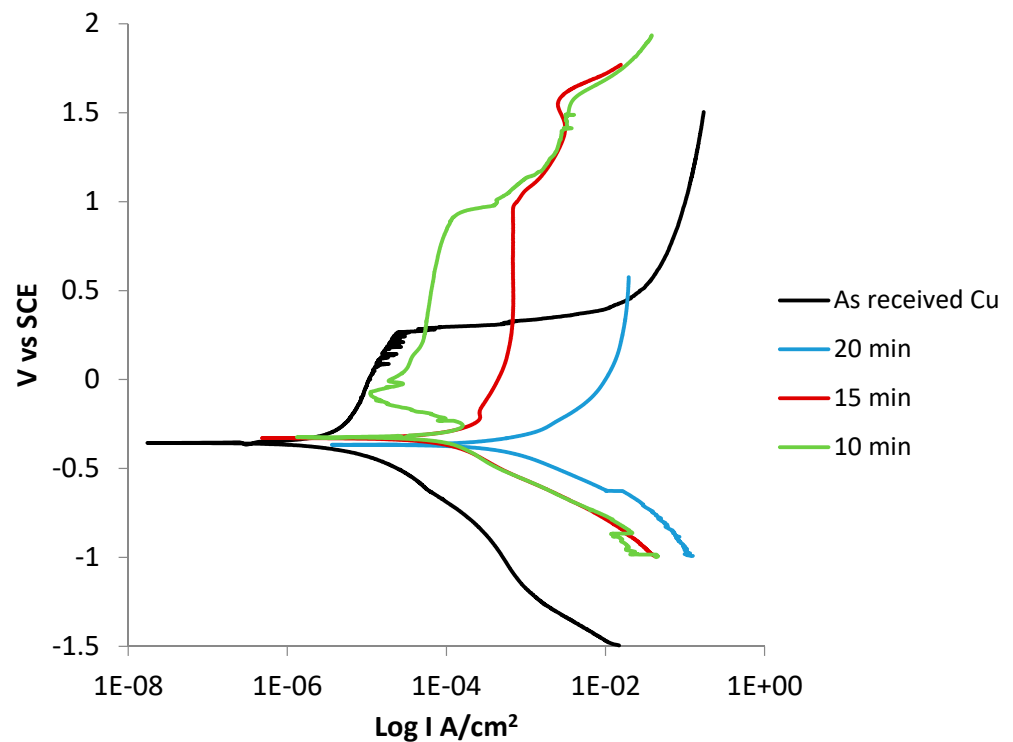


**Figure 3.** Polarization study on the as-received Cu foil and SnO<sub>2</sub>-coated Cu electrode samples deposited over different time periods in 1 M ethanol + 1 M KOH solution.

**Table 1.**  $E_{\text{corr}}$  and  $i_{\text{corr}}$  value of as received Cu and SnO<sub>2</sub>-coated Cu in 1 M ethanol + 1 M potassium hydroxide (KOH) solution.

Sample Name	$i_{\text{corr}}(\text{A}/\text{cm}^2)$	$E_{\text{corr}}(\text{V})$
As-received Cu	$3 \times 10^{-6}$	$-3.56 \times 10^{-1}$
10 min	$7 \times 10^{-5}$	$3.24 \times 10^{-1}$
15 min	$1.5 \times 10^{-4}$	$-3.29 \times 10^{-1}$
20 min	$2.5 \times 10^{-3}$	$-3.67 \times 10^{-1}$

### 3.4. EIS Analysis

The corrosion behavior of the as-received Cu and SnO<sub>2</sub>-coated Cu foil samples deposited over different time periods in 1 M ethanol + 1 M KOH solution was investigated, and mechanistic and kinetic parameters were obtained using EIS and potentiodynamic polarization techniques, and these were analyzed. Figure 4 shows the Nyquist plots obtained via the fitting of the experimental data to an equivalent circuit model, as presented in Figure 5. The fitted equivalent circuit comprises solution resistance ( $R_s$ ) between the reference electrode and working electrodes and the charge transfer resistance ( $R_{ct}$ ), which is a measure of the corrosion response at the electrolyte/metal interface [33,34]. To simulate the irregularity of metal surfaces and make the data fitting more accurate, the pure double-layer capacitance ( $C_{dl}$ ) was replaced by the constant phase element (CPE,  $Q$  as shown in the circuit in Figure 5) in the fitted circuit [35]. The corrosion resistance of different alloys can be determined from the  $R_{ct}$ , which is inversely proportional to  $i_{\text{corr}}$ . The impedance ( $Z_{\text{CPE}}$ ) of the samples can be calculated using the following expression:

$$Z_{\text{CPE}} = 1/(Y_0 (j\omega)^n)$$

where  $n$  is the phase shift exponent, the value of which ranges between 0.75 and 1.0 and indicates the CPE type (inductance, capacitance, or resistance) [36];  $\omega$  represents the angular frequency;  $j$  is the imaginary unit; and  $Y_0$  is the CPE constant.

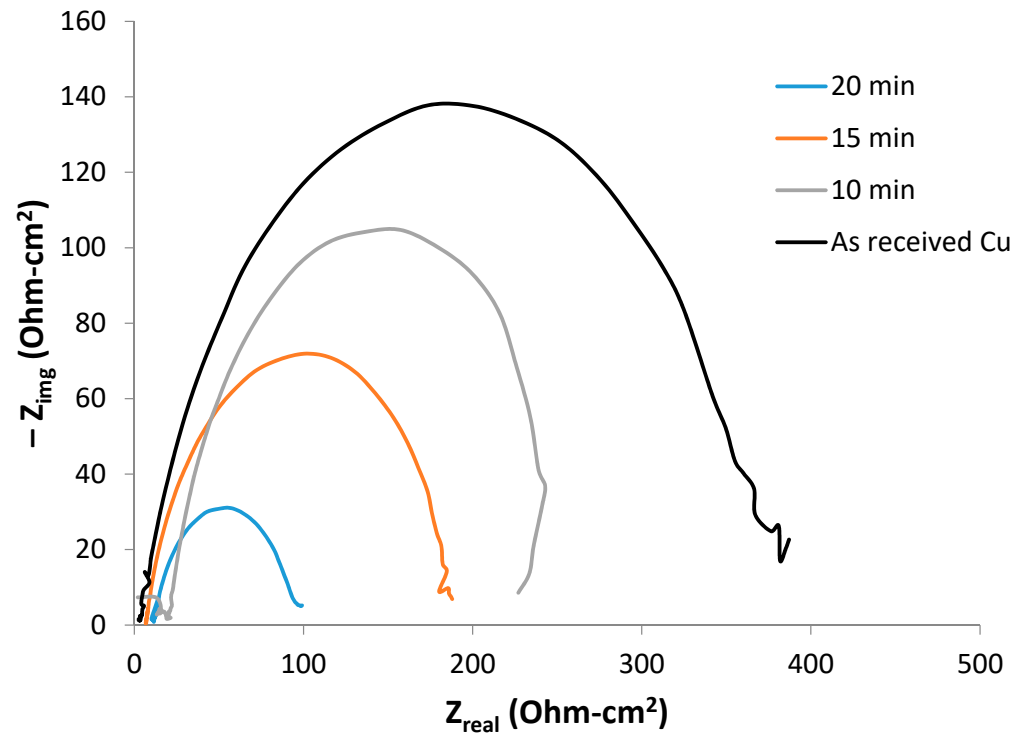


**Figure 4.** Nyquist plots of the as-received Cu and SnO<sub>2</sub>-coated Cu electrodes deposited over different time periods in 1 M ethanol + 1 M KOH solution.

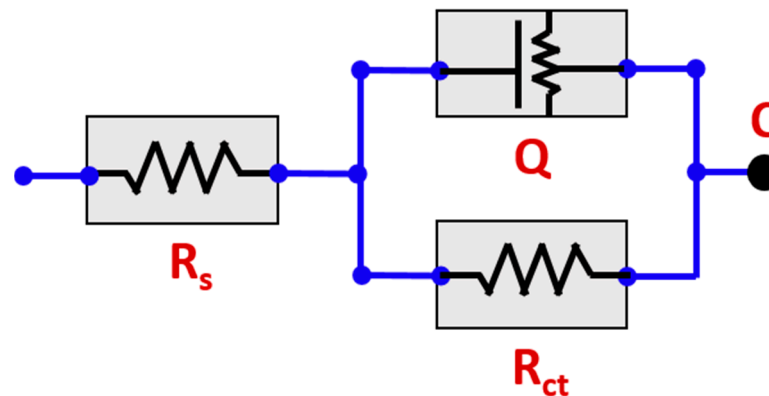


**Figure 5.** Equivalent circuit diagram.

The data extracted from the equivalent circuit are shown in Table 2.

**Table 2.** Electrochemical impedance parameters of the as-received Cu and SnO<sub>2</sub>-coated Cu electrodes deposited for different time periods in 1 M ethanol + 1 M KOH solution.

Sample Name	$R_{ct}$ (Ohm cm <sup>2</sup> )	$n$
As-received Cu	32.2	0.762
10 min	14.6	0.778
15 min	8.7	0.858
20 min	5.4	0.828

It is clear from the Nyquist plots that upon an increase in the deposition, there is a decrease in the diameter of the capacitive loop, with the smallest diameter observed for the sample with the longest deposition time of 20 min and the as-received Cu sample exhibiting the capacitive loop with the largest diameter. As previously stated, the  $R_{ct}$  value is inversely proportional to the  $i_{corr}$  value, where the values presented in Tables 1 and 2 show the same trend. The sample coated for 20 min shows the lowest  $R_{ct}$  value and thus its corrosion resistance properties, indicated by its  $i_{corr}$  value, are the worst of all the samples.

### 3.5. Materials Characterization

Figure 6 shows the PXRD patterns of the SnO<sub>2</sub>-coated Cu electrodes deposited over different time periods. All of the peaks in the patterns were indexed and identified using the matching elements function of the diffractometer library with. A tetragonal SnO<sub>2</sub> phase (JCPDS Card #41-1445) was clearly detected alongside Cu substrate peaks. Well-defined diffraction patterns were easily obtained, even at a low temperature, and their peaks assigned, indicating the formation of crystalline SnO<sub>2</sub> films, and confirming that the crystal structure of SnO<sub>2</sub> was retained after the deposition process was carried out.

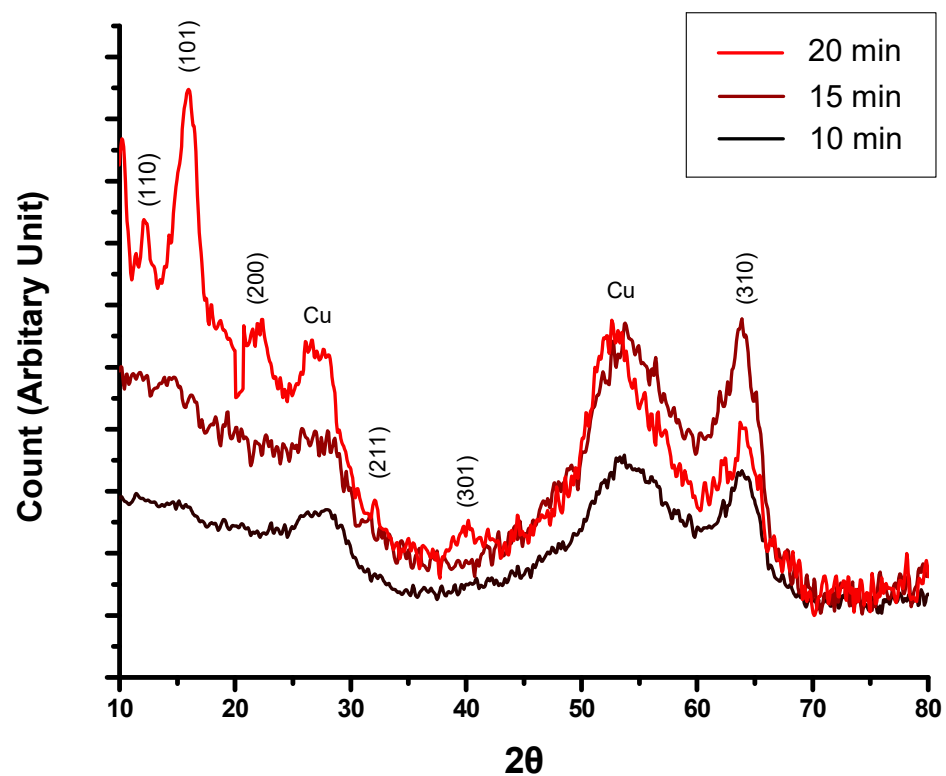
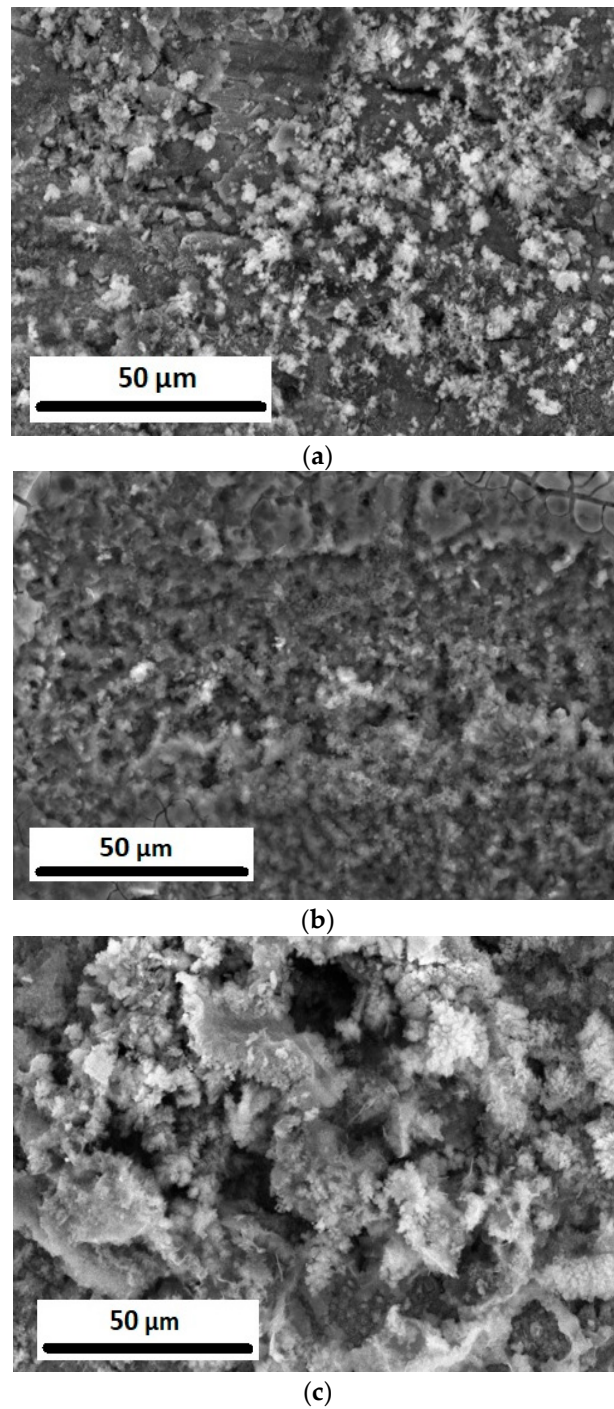


Figure 6. XRD patterns of SnO<sub>2</sub> deposited on Cu foil over different time periods.

Figure 7 shows the SEM images of the SnO<sub>2</sub>-coated Cu samples deposited over different time periods, where it can be clearly seen from the images that upon increasing the deposition time of the oxide layer on the surface of the Cu foil, the sample becomes finer. After a long deposition time, the surface becomes rougher than after a shorter time. Upon an increase in the deposition time, the fine grains in the sample aggregate to create a porous, rough surface, resulting in an increase in the current density and a subsequent increase in the  $i_{corr}$  values and the delivering of more current, which is favorable for a fuel cell.



**Figure 7.** SEM images of the SnO<sub>2</sub>-coated Cu samples deposited over (a) 10 min, (b) 15 min, and (c) 20 min.

EDX spectroscopy was used to quantitatively analyze the samples, and their Sn and O contents are presented in Table 3. The data show that the percentage of Sn increases in line with an increase in the deposition time.



**Table 3.** EDX analysis of the SnO<sub>2</sub>-coated Cu electrodes deposited over different time periods in 1 M ethanol + 1 M KOH solution.

Sample	Element	Weight%	Atom%
10 min	O	26.48	68.06
	Sn	73.52	31.94
15 min	O	20.50	63.30
	Sn	79.50	36.70
20 min	O	18.30	61.42
	Sn	81.7	38.58

#### 4. Conclusions

SnO<sub>2</sub> was deposited on Cu foil via an electrodeposition process that was carried out for different deposition times. PXRD and SEM results prove the successful formation of a SnO<sub>2</sub> film on the Cu foil, where a finer layer can be achieved by increasing the deposition time. Electrochemical analysis of the samples was carried out using CV, chronoamperometry, and potentiodynamic polarization, with the results showing that SnO<sub>2</sub>-Cu exhibits promising efficiency to be an economical, high-performance, and excellent electrode material for use in electrocatalytic fuel cells. This electrode material is much cheaper than the expensive commercial Pt electrodes currently available, which are most commonly used in direct ethanol fuel cells. This present investigation opens up a new avenue for the commercial and economical production of renewable energy using fuel cells powered by bio ethanol from biomass. The results of this work thus provide strong incentive and serve to encourage the research on and manufacturing of fuel cells for commercial purposes to move to a new level of innovation based on the low-cost quality concept presented here.

**Author Contributions:** Conceptualization, H.S.A. and A.H.S.; data curation, A.S., M.G., S.S., and J.A.M.; formal analysis, A.H.S., S.A.R., and A.S.; funding acquisition, A.H.S.; investigation, H.S.A. and A.S.; methodology, M.G., S.S., and H.S.A.; resources, A.H.S.; software, H.S.A.; supervision, H.S.A.; validation, A.S., S.A.R., and J.A.M.; visualization, S.S.; writing—original draft, H.S.A. and A.H.S.; writing—review and editing, H.S.A. All authors have read and agreed to the published version of the manuscript.

**Funding:** This work was funded by the Deputyship for Research & Innovation, “Ministry of Education” in Saudi Arabia through the project number IFKSURG-1439-029.

**Institutional Review Board Statement:** Not applicable.

**Informed Consent Statement:** Not applicable.

**Data Availability Statement:** The data presented in this study are available on request from the corresponding author.

**Acknowledgments:** The authors extend their appreciation to the Deputyship for Research & Innovation, “Ministry of Education” in Saudi Arabia for funding this research work through the project number IFKSURG-1439-029.

**Conflicts of Interest:** The authors declare no conflict of interest.

#### References

1. Agnihotri, O.; Mohammad, M.; Abass, A.; Arshak, K. Electrical and optical properties of chemically deposited conducting glass for SIS solar cells. *Solid State Commun.* **1983**, *47*, 195–198. [[CrossRef](#)]
2. Summitt, R.; Marley, J.A.; Borrelli, N.F. The ultraviolet absorption edge of stannic oxide (SnO<sub>2</sub>). *J. Phys. Chem. Solids* **1964**, *25*, 1465–1469. [[CrossRef](#)]
3. Ginley, D.S.; Bright, C. Transparent Conducting Oxides. *MRS Bull.* **2000**, *25*, 15–18. [[CrossRef](#)]
4. Ginley, D.; Coutts, T.; Perkins, J.; Young, D.; Li, X.; Parilla, P. Next-Generation Transparent Conducting Oxides for Photovoltaic Cells: An Overview. In Proceedings of the MRS Online Proceedings Library, England, UK, January 2001; Volume 668, p. 27. [[CrossRef](#)]

5. Hartnagel, H.L.; Dawar, A.L.; Jain, A.K.; Jagadish, C.J. *Semiconducting Transparent Thin Films*; CRC Press, IOP: Bristol, UK, 1995; ISBN 10: 9780750303224.
6. Shoyama, M.; Hashimoto, N. Effect of poly ethylene glycol addition on the microstructure and sensor characteristics of SnO<sub>2</sub> thin films prepared by sol-gel method. *Sens. Actuators B Chem.* **2003**, *93*, 585–589. [[CrossRef](#)]
7. Chang, S.; Leu, I.-C.; Hon, M. Electrodeposition of nanocrystalline SnO<sub>2</sub> coatings with two-layer microstructure. *J. Cryst. Growth* **2004**, *273*, 195–202. [[CrossRef](#)]
8. Yuan, X.; Cao, L.; Wan, H.; Zeng, G.; Xi, S. Study on the self-packing of SnO<sub>2</sub> nanoparticles at the air-hydrosol interface and its composite LB films with arachidic acid. *Thin Solid Film.* **1998**, *327–329*, 33–36. [[CrossRef](#)]
9. Santos, L.R.B.; Chartier, T.; Pagnoux, C.; Baumard, J.F.; Santillii, C.V.; Pulcinelli, S.H.; Larbot, A. Tin oxide nanoparticle formation using a surface modifying agent. *J. Eur. Ceram. Soc.* **2004**, *24*, 3713–3721. [[CrossRef](#)]
10. Udawatte, C.P.; Kakihana, M.; Yoshimura, M. Preparation of pure perovskite-type BaSnO<sub>3</sub> powders by the polymerized complex method at reduced temperature. *Solid State Ion.* **1998**, *108*, 23–30. [[CrossRef](#)]
11. Sergent, N.; Gélin, P.; Périer-Camby, L.; Pralraud, H.; Thomas, G. Preparation and characterisation of high surface area stannic oxides: Structural, textural and semiconducting properties. *Sens. Actuators B Chem.* **2002**, *84*, 176–188. [[CrossRef](#)]
12. Ibarguen, C.A.; Mosquera, A.; Parra, R.; Castro, M.; Rodríguez-Páez, J. Synthesis of SnO<sub>2</sub> nanoparticles through the controlled precipitation route. *Mater. Chem. Phys.* **2007**, *101*, 433–440. [[CrossRef](#)]
13. Cullity, B.D.; Weymouth, J.W. Elements of X-Ray Diffraction. *Am. J. Phys.* **1957**, *25*, 394–395.
14. Izaki, M.; Omi, T. Electrolyte Optimization for Cathodic Growth of Zinc Oxide Films. *J. Electrochem. Soc.* **1996**, *143*, L53–L55. [[CrossRef](#)]
15. Peulon, S.; Lincot, D. Cathodic electrodeposition from aqueous solution of dense or open-structured zinc oxide films. *Adv. Mater.* **1996**, *8*, 166–170. [[CrossRef](#)]
16. Zhitomirsky, I.; Gal-Or, L.; Kohn, A.; Hennicke, H.W. Electrodeposition of ceramic films from non-aqueous and mixed solutions. *J. Mater. Sci.* **1995**, *30*, 5307–5312. [[CrossRef](#)]
17. Bohannan, E.W.; Jaynes, C.C.; Shumsky, M.G.; Barton, J.K.; Switzer, J.A. Low-temperature electrodeposition of the high-temperature cubic polymorph of bismuth(III) oxide. *Solid State Ion.* **2000**, *131*, 97–107. [[CrossRef](#)]
18. Yao, J.; Chen, P.; Fujishima, A. Electrochromic behavior of electrodeposited tungsten oxide thin films. *J. Electroanal. Chem.* **1996**, *406*, 223–226. [[CrossRef](#)]
19. Dierstein, A.; Natter, H.; Meyer, F.; Stephan, H.-O.; Kropf, C.; Hempelmann, R. Electrochemical deposition under oxidizing conditions (EDOC): A new synthesis for nanocrystalline metal oxides. *R. Scr. Mater.* **2001**, *44*, 2209–2212. [[CrossRef](#)]
20. Chang, S.T.; Leu, I.C.; Hon, M.H. Preparation and characterization of nanostructured tin oxide films by electrochemical deposition. *Electrochem. Solid-State Lett.* **2002**, *5*, C71–C74. [[CrossRef](#)]
21. Zheng, M.; Li, G.; Zhang, X.; Huang, S.; Lei, Y.; Zhang, L. Fabrication and structural characterization of large-scale uniform SnO<sub>2</sub> nanowire array embedded in anodic alumina membrane. *Chem. Mater.* **2001**, *13*, 3859–3861. [[CrossRef](#)]
22. Zhitomirsky, I. Cathodic electrodeposition of ceramic and organoceramic materials. *Fundam. Asp. Adv. Colloid Interface Sci.* **2002**, *97*, 279–317. [[CrossRef](#)]
23. Abdo, H.S.; Sherif, E.-S.M.; El-Serehy, H.A. Manufacturing of Ti-6%Al and Ti-6%Al-4%V Alloys and Their Corrosion in Sodium Chloride Solutions. *Crystals* **2020**, *10*, 181. [[CrossRef](#)]
24. Pauporté, T.; Lincot, D. Electrodeposition of semiconductors for optoelectronic devices: Results on zinc oxide. *Electrochim. Acta* **2000**, *45*, 3345–3353. [[CrossRef](#)]
25. Qiu, X.-F.; Zhu, J.-J.; Chen, H.-Y. Controllable synthesis of nanocrystalline gold assembled whiskery structures via sonochemical route. *J. Cryst. Growth* **2003**, *257*, 378–383. [[CrossRef](#)]
26. Li, N.; Charles, R. Martin and Bruno Scrosati, A High-Rate, High-Capacity, Nanostructured Tin Oxide Electrode. *Electrochem. Solid State Lett.* **2000**, *3*, 316. [[CrossRef](#)]
27. Zhang, X.; Liu, Y.-C.; Zhang, J.; Lu, Y.; Shen, D.; Fan, X.; Kong, X. Structure and photoluminescence of Mn-passivated nanocrystalline ZnO thin films. *J. Cryst. Growth* **2003**, *254*, 80–85. [[CrossRef](#)]
28. Baik, N.S.; Sakai, G.; Shimano, K.; Miura, N.; Yamazoe, N. Hydrothermal treatment of tin oxide sol solution for preparation of thin-film sensor with enhanced thermal stability and gas sensitivity. *Sens. Actuators B Chem.* **2000**, *65*, 97–100. [[CrossRef](#)]
29. Singh, A.; Aswal, D.K.; Viswanadham, C.; Goswami, G.; Gupta, L.; Gupta, S.; Yakhmi, J.V. Enhanced magnetoresistance in nanocrystalline La<sub>0.6</sub>Pb<sub>0.4</sub>MnO<sub>3</sub> thin films. *J. Cryst. Growth* **2002**, *244*, 313–317. [[CrossRef](#)]
30. Chavez, K.L.; Hess, D.W. A Novel Method of Etching Copper Oxide Using Acetic Acid. *J. Electrochem. Soc.* **2001**, *148*, G640–G643. [[CrossRef](#)]
31. Zhao, L.; Mitsushima, S.; Ishihara, A.; Matsuzawa, K.; Ota, K.-I. Pt-Ir-SnO<sub>2</sub>/C Electrocatalysts for Ethanol Oxidation in Acidic Media. *Chin. J. Catal.* **2011**, *32*, 1856–1863. [[CrossRef](#)]
32. Abdo, H.S.; Seikh, A.H.; Mohammed, J.A.; Luqman, M.; Ragab, S.A.; Almotairy, S.M. Influence of Chloride Ions on Electrochemical Corrosion Behavior of Dual-Phase Steel over Conventional Rebar in Pore Solution. *Appl. Sci.* **2020**, *10*, 4568. [[CrossRef](#)]
33. Abdo, H.S.; Seikh, A.H.; Mandal, B.B.; Mohammed, J.A.; Ragab, S.A.; Abdo, M.S. Microstructural Characterization and Corrosion-Resistance Behavior of Dual-Phase Steels Compared to Conventional Rebar. *Crystals* **2020**, *10*, 1068. [[CrossRef](#)]
34. Singh, A.K.; Shukla, S.K.; Singh, M.; Quraishi, M. Inhibitive Effect of Ceftazidime on Corrosion of Mild Steel in Hydrochloric Acid Solution. *Mater. Chem. Phys.* **2011**, *129*, 68–76. [[CrossRef](#)]

- 
35. El Azhar, M.; Mernari, B.; Traisnel, M.; Bentiss, F.; Lagrenée, M. Corrosion Inhibition of Mild Steel by the New Class of Inhibitors [2,5- Bis(n-Pyridyl)-1,3,4-Thiadiazoles] in Acidic Media. *Corros. Sci.* **2001**, *43*, 2229–2238. [[CrossRef](#)]
  36. Macdonald, J.R.; Johnson, W.B. *Impedance Spectroscopy: Theory, Experiment, and Applications*, 2nd ed.; Wiley: New York, NY, USA, 1987; ISBN 978-0-471-64749-2.